Electronic Supplementary Material (ESI) for Physical Chemistry Chemical Physics.

Exploring Cycling Induced Crystallographic Change in NMC with X-ray Diffraction Computed Tomography

Sohrab R. Daemi, Chun Tan, Antonis Vamvakeros, Thomas M. M. Heenan, Donal P. Finegan, Marco Di Michiel, Andrew M. Beale, James Cookson, Enrico Petrucco, Julia S. Weaving, Simon Jacques, Rhodri Jervis, Dan J. L. Brett, Paul R. Shearing**

1. Supplementary Results

1.1. Percentage of Discharge Capacity Loss

The percentage of discharge capacity loss for each cell between the first cycle after formation and last cycles are presented in **Table S 1**. The electrode is lithiated as a last step before cell disassembly.

Table S 1: Percentage of discharge capacity loss calculated between the first and last cycles.

Cells (4.2 V)	% Discharge Cap. Loss	Cells (4.7 V)	% Discharge Cap. Loss
42-25	1.3	47-25	15.4
42-50	13.1	47-50	26.8
42-75	0.8	47-75	35.1
42-100-1	23.3	47-100-1	56.7
42-100-2	24.4	47-100-2	52.7

1.2. ROI Lattice Parameter Maps

The ROI maps for the *a* and *c* lattice parameters and *V* are presented in **Figure S 1** for 42-100-2.

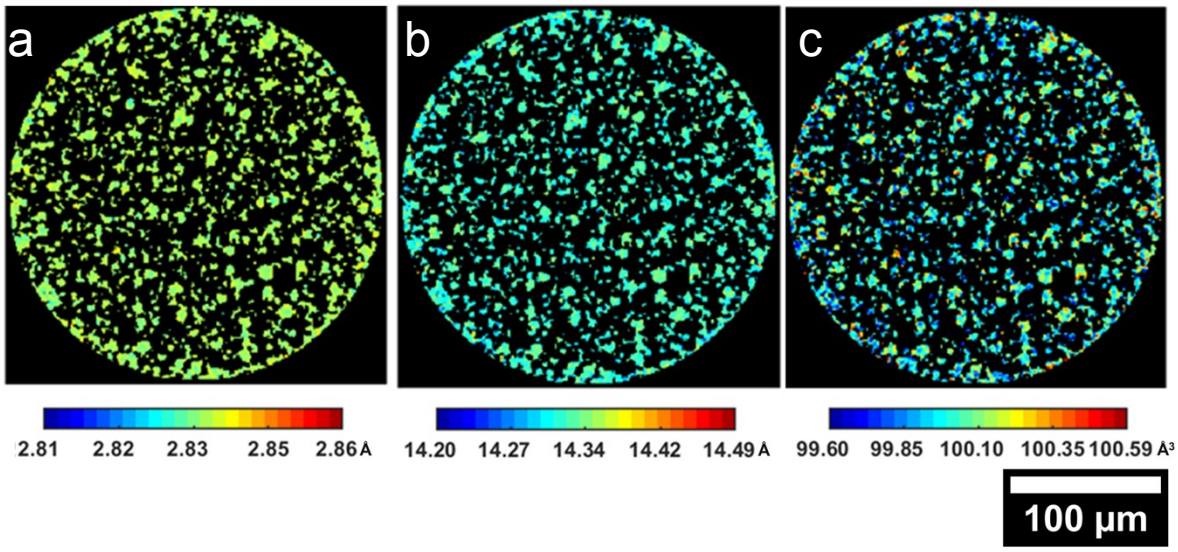

Figure S 1: Lattice parameter maps for the a) *a*, b) *c* and c) *V* for the 42-100-2 electrode.

The ROI maps for the *a* and *c* lattice parameters and *V* are presented in **Figure S 2** for 47-100-2.

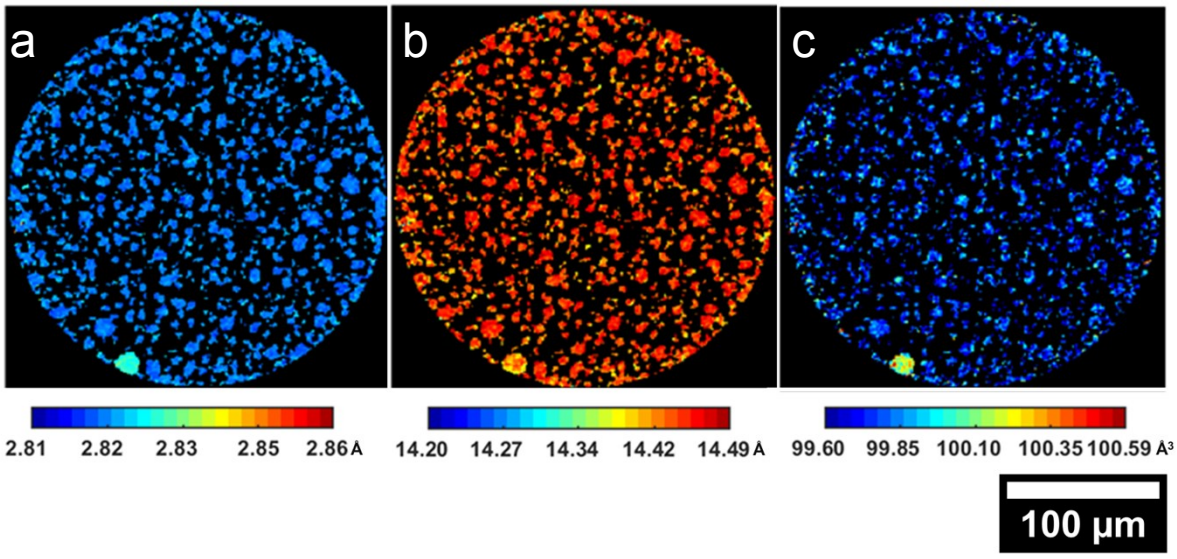

Figure S 2: Lattice parameter maps for the a) *a*, b) *c* and c) *V* for the 47-100-2 electrode.

A particle with a different lattice parameter to the bulk of the electrode can be observed in **Figure S 2**. The average lattice parameters for each of the electrode slices and values from literature are presented in **Table S 2**.

Table S 2: Average lattice dimensions for the electrodes cycled to 4.2 V and 4.7 V.

Number of cycles	*a* (Å)	*c* (Å)	*V* (Å^3)	*a* (Å)	*c* (Å)	*V* (Å^3)
Uncycled	2.856	14.221	100.442	-	-	-
Uncycled (Literature)[24]	2.86	14.25	100.5	-	-	-
	4.2 V			***4.7 V***		
25	2.847	14.266	100.248	2.842	14.319	100.149
50	2.845	14.284	100.123	2.844	14.318	100.298
75	2.849	14.262	100.255	2.844	14.310	100.235
100-1	2.843	14.290	100.064	2.829	14.416	99.941
100-2	2.839	14.325	99.989	2.824	14.437	99.718

1.3. Lattice Parameter Radial Depth Distribution

The plots for the ratio of the lattice parameter and the mean particle lattice parameter with increasing distance within the particle are presented in **Figure S 3** for the electrodes cycled to 4.2 V and **Figure S 4** for the electrodes cycled to 4.7 V.

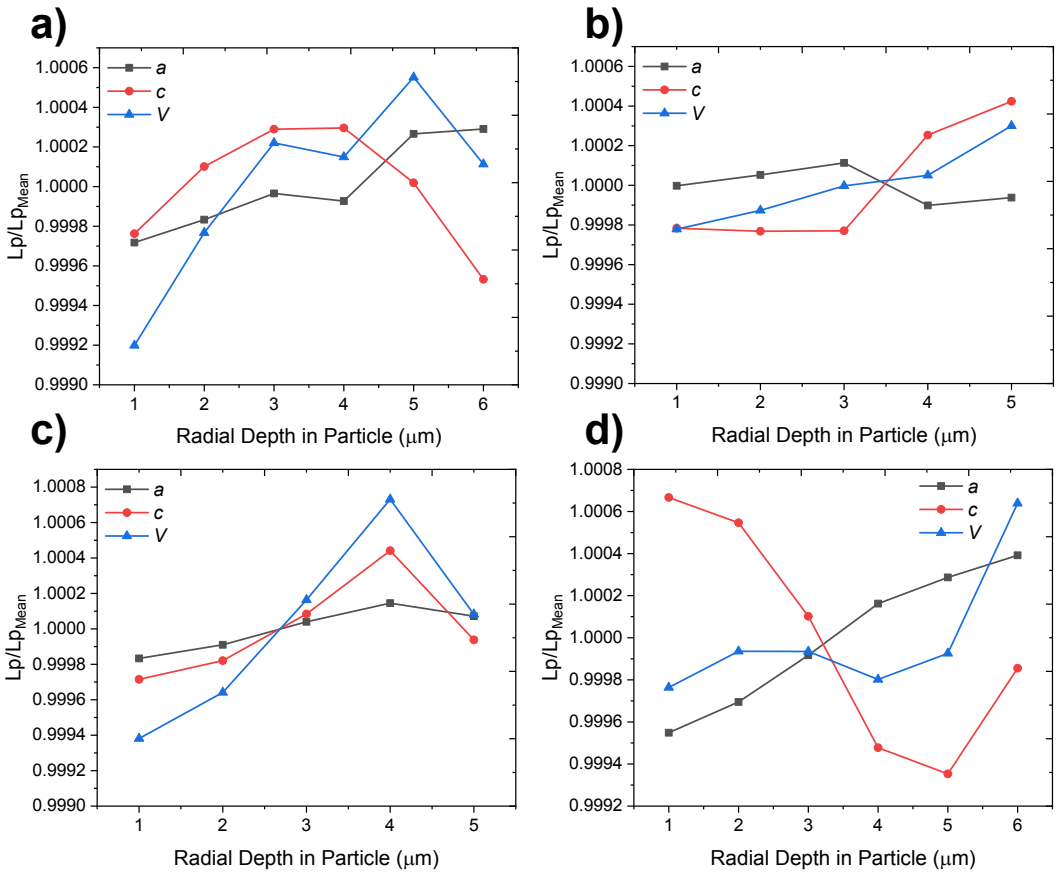

Figure S 3: Ratio between lattice parameter and mean particle lattice parameter vs. radial depth in particle calculated with a Euclidean distance map for a) uncycled electrode b) 42-25, c) 42-100-1 and d) 42-100-2.

As the plots demonstrate, there is no recognizable trend as the lattice parameter is measured towards the core of the particle.

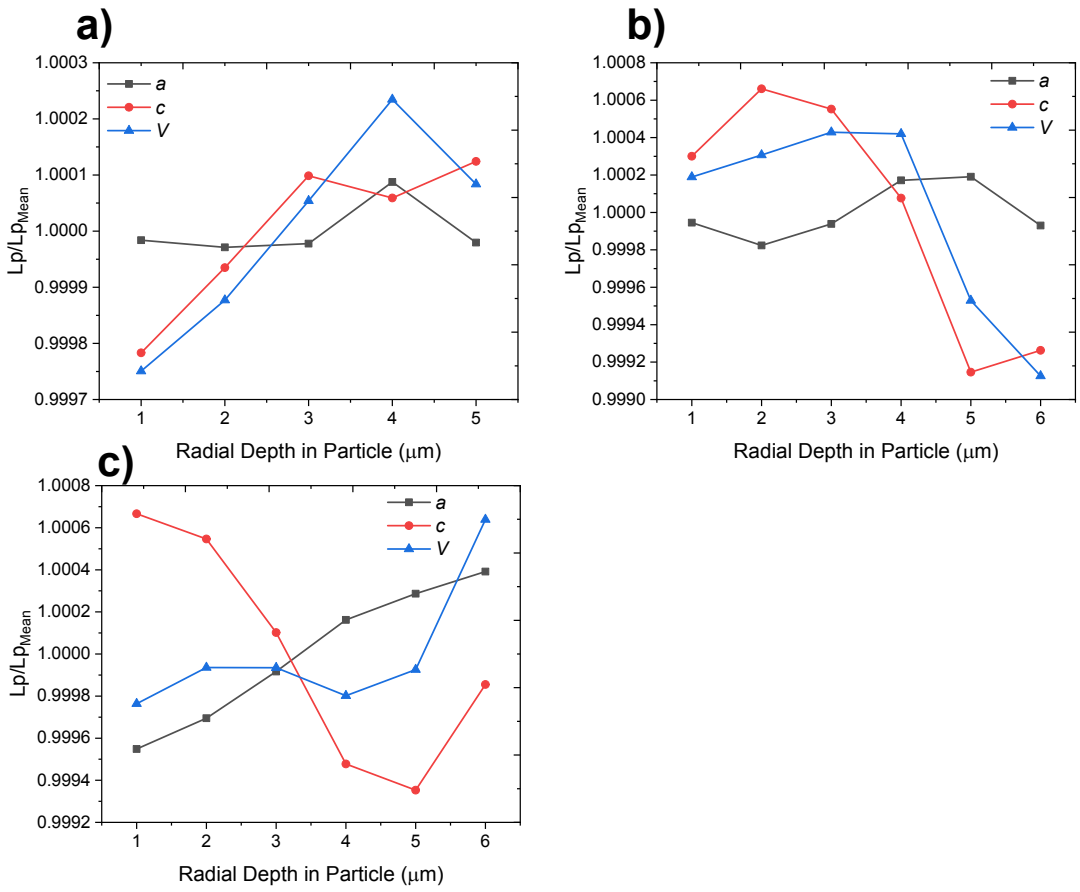

Figure S 4: Ratio between lattice parameter and mean particle lattice parameter vs. radial depth in particle calculated with a Euclidean distance map for a) 47-25, b) 47-100-1 and c) 47-100-1.

2. Supplementary Methods

2.1. Rietveld Refinement

The Rietveld refinement analysis of the XRD-CT data presented herein was based on the intensity of the scale factors and as such it is treated as a semi-quantitative analysis. In order to have a good starting model, the summed diffraction pattern of each XRD-CT dataset (i.e. reconstructed data volume) was exported and then quantitative Rietveld analysis was performed. Two phases were included in the model; $Li(Ni_{1/3}Co_{1/3}Mn_{1/3})O_2$ (ICSD: 259697) and Al (ICSD: 43423). Initially, the parameters refined were the background (2nd degree Chebyshev polynomial), scale factors and lattice parameters for both phases. In the following step, the thermal parameters of NMC were refined along with the z position of the oxygen atom. A constraint was applied setting the thermal parameters of Ni, Mn and Co to be equal and their value to be the lower limit for Li and O. This led to very stable refinements and good fits as

presented hereafter. The observed and calculated curves for the electrodes cycled to 4.2 V are presented in **Figure S 5**.

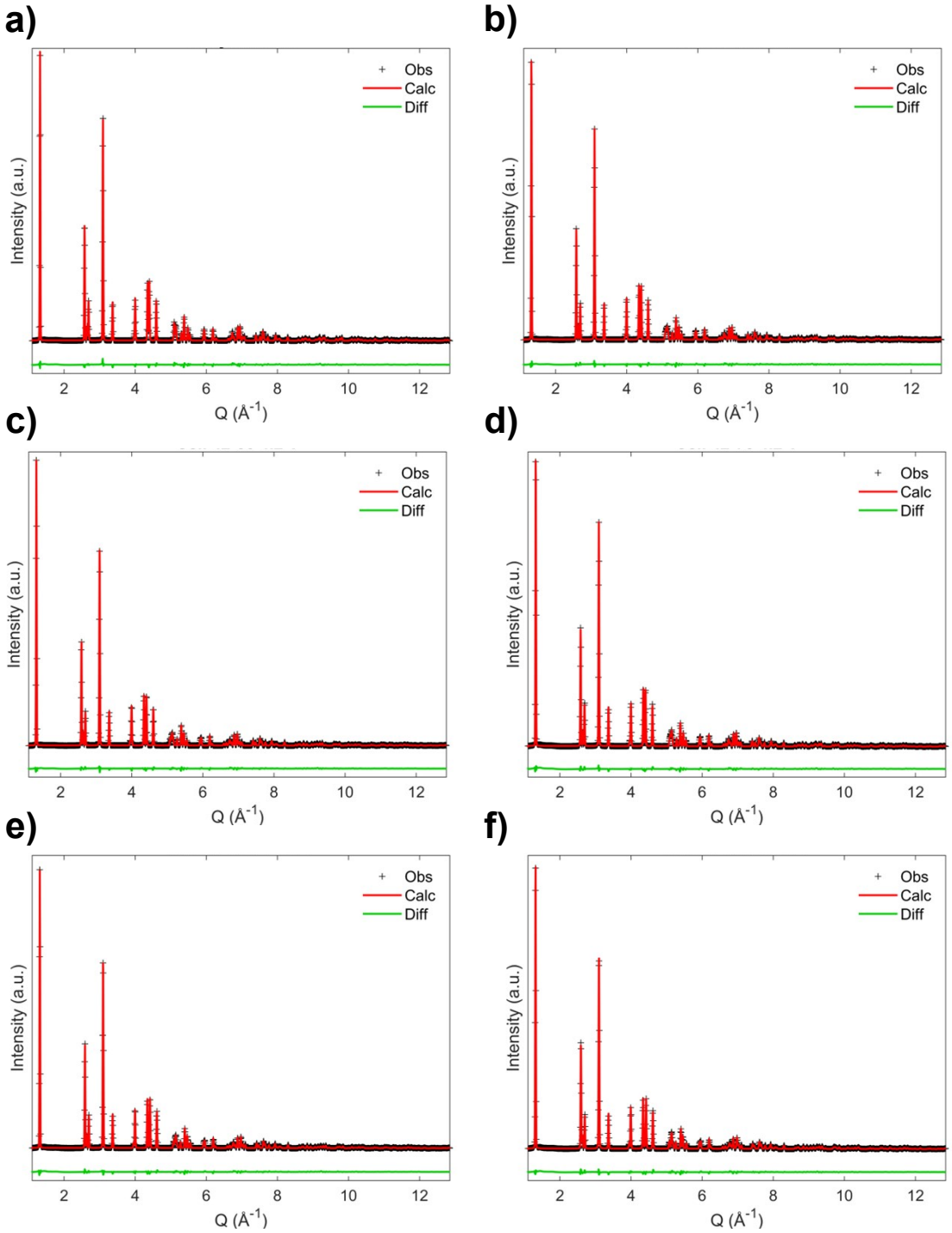

Figure S 5: Observed versus calculated curves for the a) uncycled, b) 42-25, c) 42-50, d) 42-75, e) 42-100-1 and f) 42-100-2 electrodes.

The magnified diffraction patterns for the electrodes cycled to 4.2 V can be viewed in **Figure S 6.**

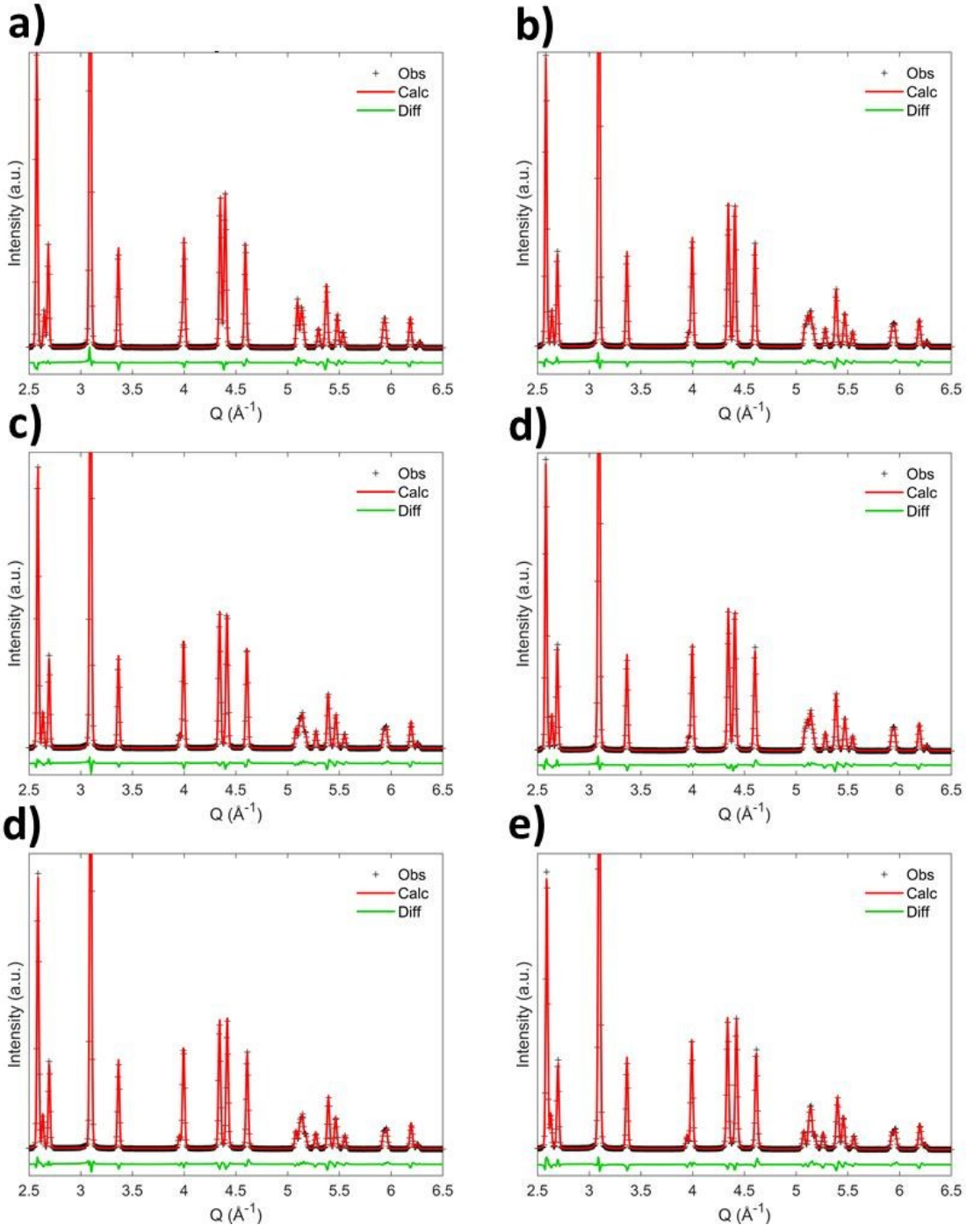

Figure S 6: Magnified diffraction patterns for the a) uncycled, b) 42-25, c) 42-50, d) 42-75, e) 42-100-1 and f) 42-100-2 electrodes.

The observed and calculated curves for the electrodes cycled to 4.7 V are presented in **Figure S 7**.

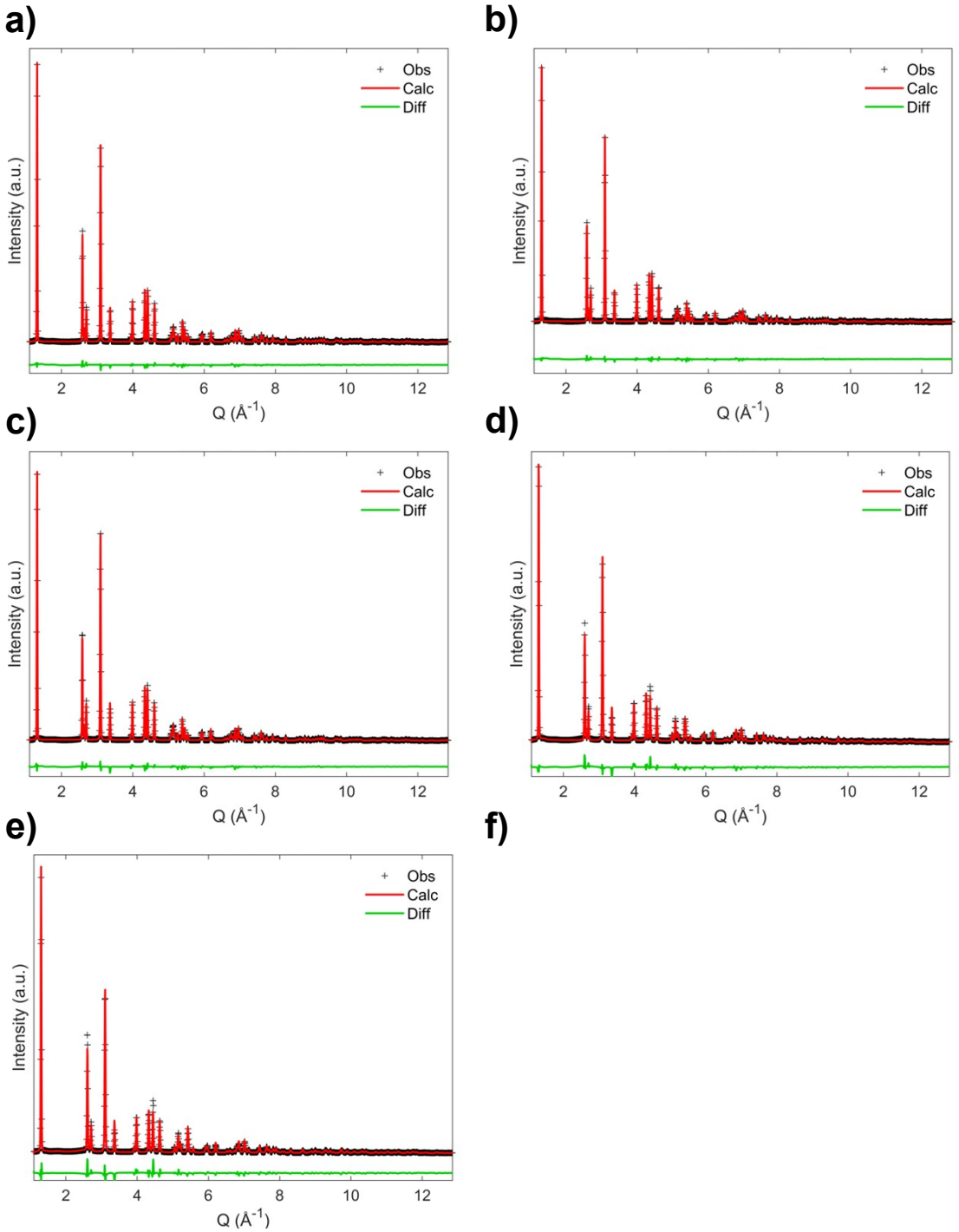

Figure S 7: Observed versus calculated curves for the a) uncycled, b) 47-25, c) 47-50, d) 47-75, e) 47-100-1 and f) 47-100-2 electrodes.

The magnified diffraction patterns for the electrodes cycled to 4.7 V can be viewed in **Figure S 8.**

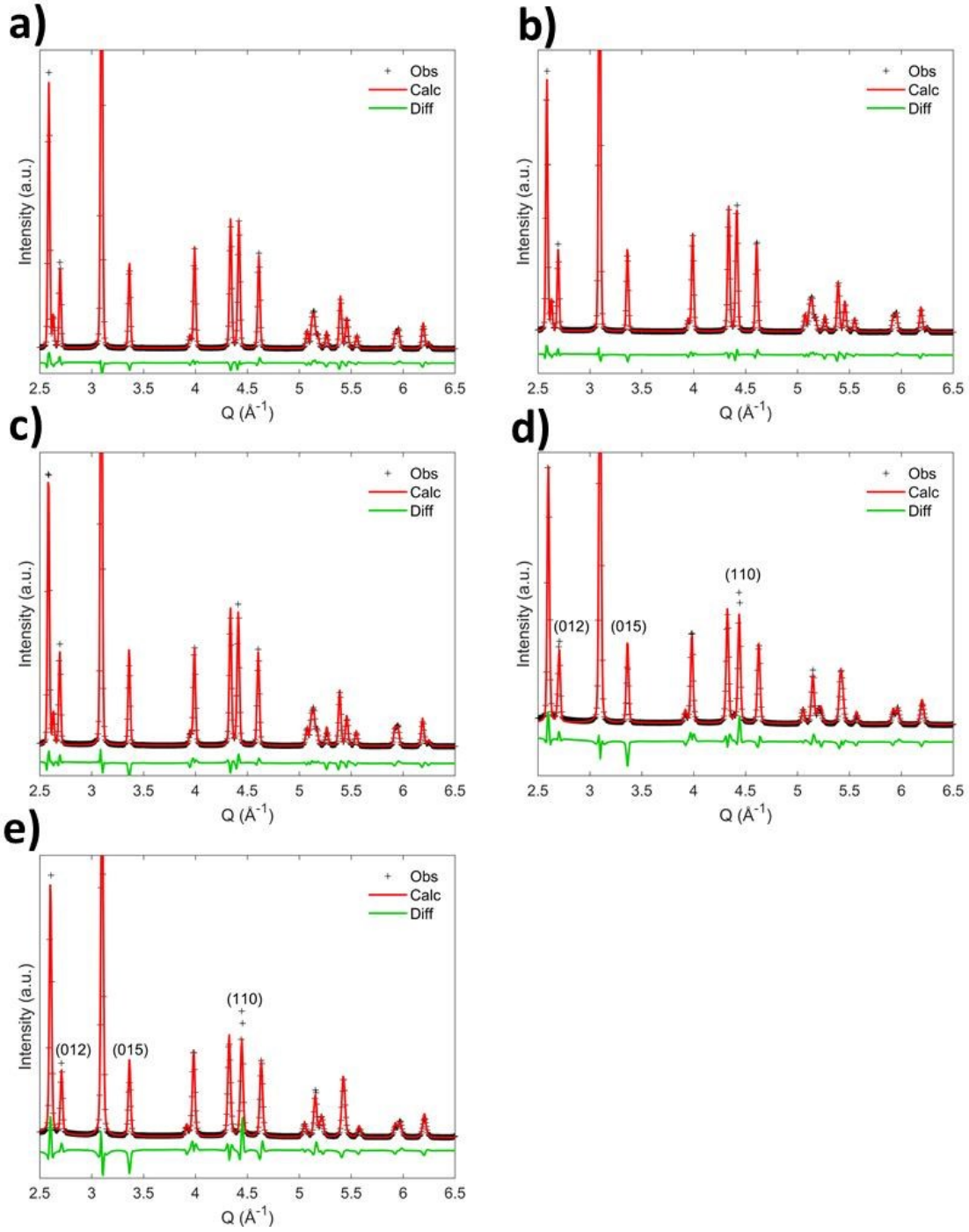

Figure S 8: Magnified diffraction patterns for the a) uncycled, b) 47-25, c) 47-50, d) 47-75, e) 47-100-1 and f) 47-100-2 electrodes.

As a final step, the mild broadening of the NMC peaks was modelled by refining strain (it yielded significantly better results than the crystallite size refinement). This process was repeated for the summed diffraction pattern of each XRD-CT dataset yielding a good starting model for the batch analysis of the spatially-resolved XRD-CT data. For each XRD-CT dataset, the

respective model was used and the following parameters were refined: background (2nd degree Chebyshev polynomial), scale factors and lattice parameters for NMC and Al phases (it was found that refining the thermal parameters, occupancy of the various atoms and/or strain led to unstable refinements). The weighted-profile R (RWP) values for the refinement are presented in **Table S 3**. As explained in the main text, a higher RWP may indicate the formation of new phases for the electrodes cycled to 4.7 V.

Table S 3: RWP values for the Rietveld refinement.

Electrode (4.2 V)	RWP (%)	Electrode (4.7 V)	RWP (%)
Uncycled	**2.59**	**-**	**-**
42-25	**2.11**	**47-25**	**3.02**
42-50	**2.15**	**47-50**	**2.71**
42-75	**2.49**	**47-75**	**3.79**
42-100-1	**2.51**	**47-100-1**	**6.27**
42-100-2	**2.49**	**47-100-2**	**8.09**

To gauge whether any cation intermixing has occurred as a result of cycling at higher voltages, the ratio between the (0 0 3)/(1 0 4) peak intensities was calculated and presented in **Table S 4.**

Table S 4: The ratios of the (0 0 3)/(1 0 4) peak intensities and associated RWP value.

Electrode (4.2 V)	Intensity Ratio	RWP (%)	Electrode (4.7 V)	Intensity Ratio	RWP (%)
Uncycled	1.28	1.18	**-**		**-**
42-25	1.31	1.29	**47-25**	1.47	1.44
42-50	1.48	1.17	**47-50**	1.42	1.18
42-75	1.48	1.19	**47-75**	1.37	1.21
42-100-1	1.27	1.59	**47-100-1**	1.36	1.84
42-100-2	1.50	1.26	**47-100-2**	1.54	2.4

These were calculated using a pseudo-Voigt model with Topas with excellent resulting RWP values.

2.2.

2.3. Lattice Parameter Map Masking and Analysis

The Rietveld refinement outputs a continuous lattice parameter map, as the lattice parameter of small particle fragments with weaker diffraction signals are also resolved in the image. A masking procedure, detailed hereafter, was hence devised to localize the lattice parameter to the particle using custom MATLAB® (Mathworks, Version R2015a) scripts. To obtain the particle masks, the initial diffraction intensity images, output directly after integration and reconstruction, were imported into MATLAB, where these were transformed into a mask with the *imbinarize* MATLAB® function. The diffraction intensity image and the resulting mask are presented **Figure S 9** in a-b). The mask is successively superimposed on the continuous lattice parameter data, with the map of the *a* lattice parameter shown in Figure S 9 c) generating a discrete localized lattice parameter map, shown in Figure S 9 d). This map allows identification of the lattice parameter values internal to the particles. While the overall resolution does not allow resolving finer microstructural features, it is sufficient to isolate large particles for further analysis.

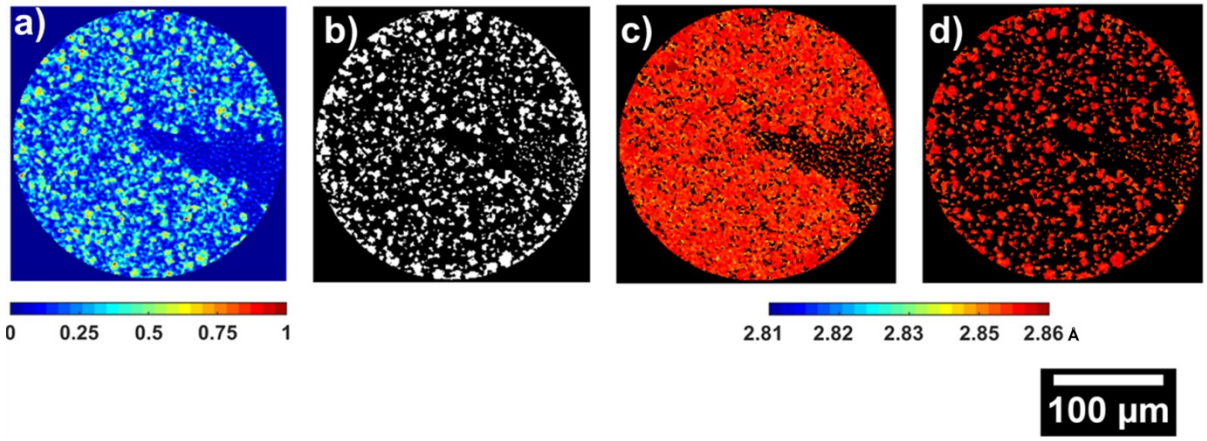

Figure S 9: a) Mean diffraction intensity image from the uncycled electrode. Colour bar in arbitrary units (arb. units). b) Binary mask obtained by thresholding the mean diffraction intensity image in a). c) Continuous map of a lattice parameter obtained after refinement and d) its masked version.

To further study the lattice parameter distribution within individual particles, an algorithm to measure the intra-particle variation of the lattice parameter was devised. This algorithm uses the MATLAB® bwdist function to generate the Euclidean distance map within each particle, shown in **Figure S 10**. This allows calculating the average lattice parameter for increasing distance within the particle.

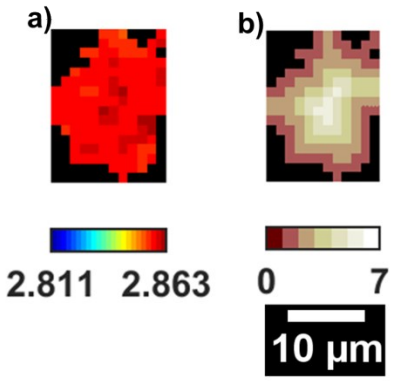

Figure S 10: a) Individual particle extracted from the uncycled dataset. b) The Euclidean distance map. Colour bars in Å and µm respectively.

Both the electrode ROI and single particle datasets are processed using the above procedure the *a* and *c* lattice parameters and the lattice unit volume (*V*). The images are plotted with MATLAB and modified with ImageJ.

The lattice parameters are averaged for the full electrode scans. The standard error (SE) of the average lattice parameter was calculated via the equation:

$$SE = \frac{standard\ deviation}{\sqrt{sample\ size}} \qquad (1)$$

The error was calculated to be below 0.00002 Å for the lattice parameters and 0.002 Å^3 for the *V* so is regarded as negligible for this study.

2.4. FIB-SEM Imaging

For completeness, additional FIB-SEM cross sections are presented in the following figures. **Figure S 11** contains the slices gathered from the uncycled electrode. Very few cracks can be observed inside the particles.

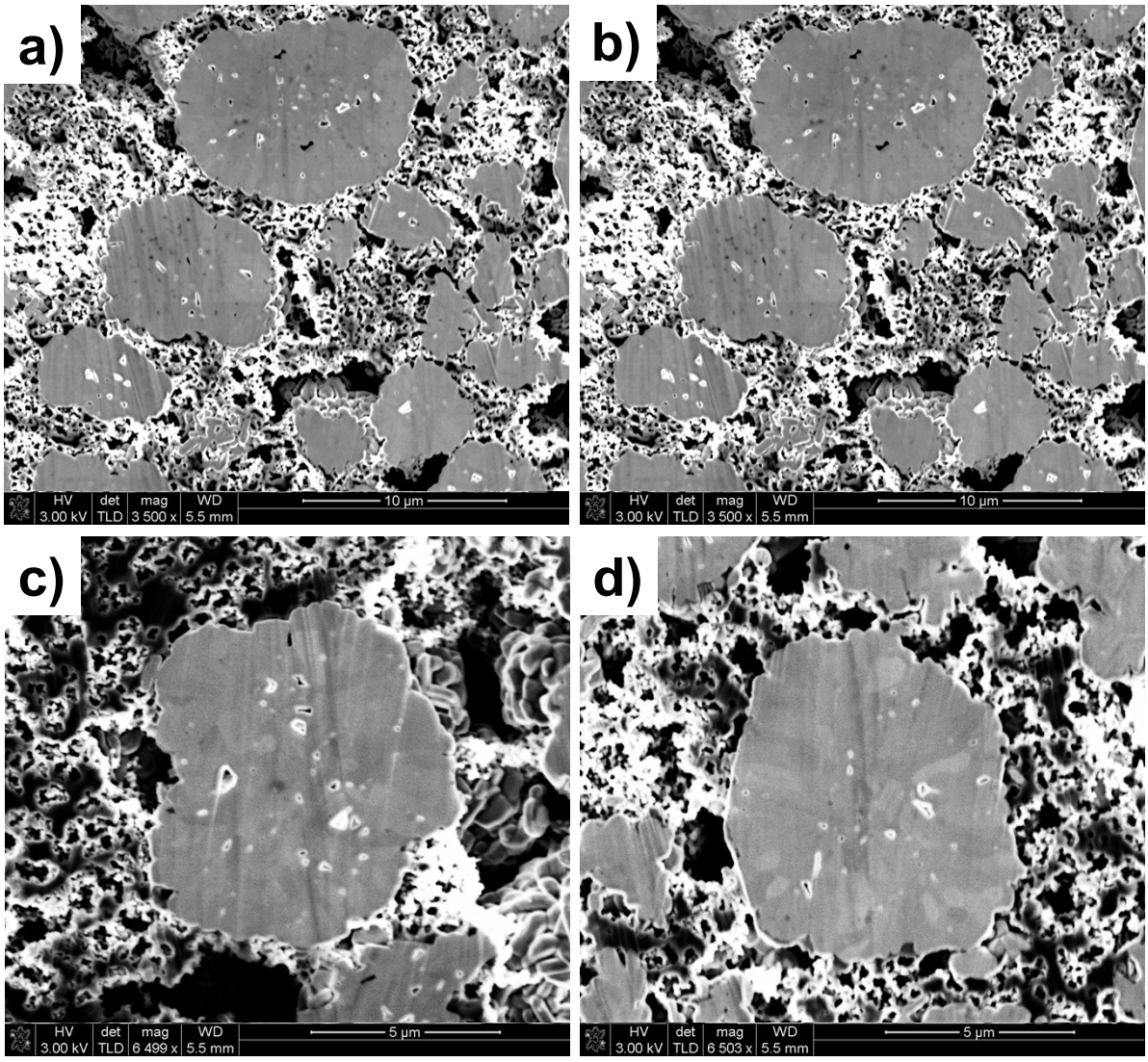

Figure S 11: FIB-SEM cross-sectional slices of the a-b) uncycled electrode taken at 3.5 k× and c-d) uncycled particle taken at 6.5 k×.

Figure S 12 presents cross-sectional slices taken from the 42-100-1 electrode. Cracks can be seen originating at the core of the particle and extending towards the surface.

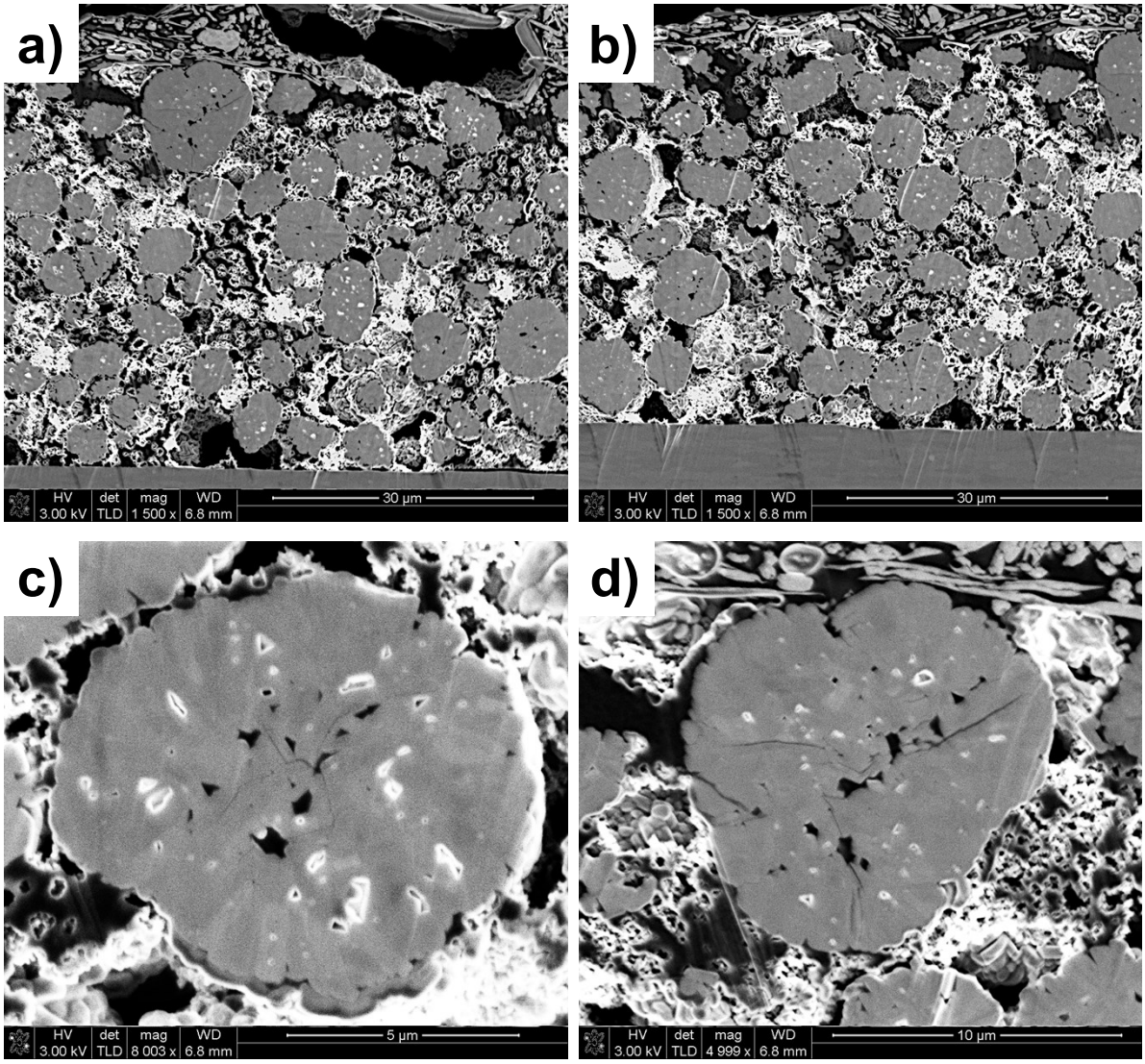

Figure S 12: FIB-SEM cross-sectional slices of a-b) the 42-100-1 electrode taken at 1.5 k× and c-d) two particles taken at 8 k×.

Figure S 13 presents cross-sectional slices taken from the 47-100-1 electrode. Cracks can be seen originating at the core of the particle and propagating towards the surface.

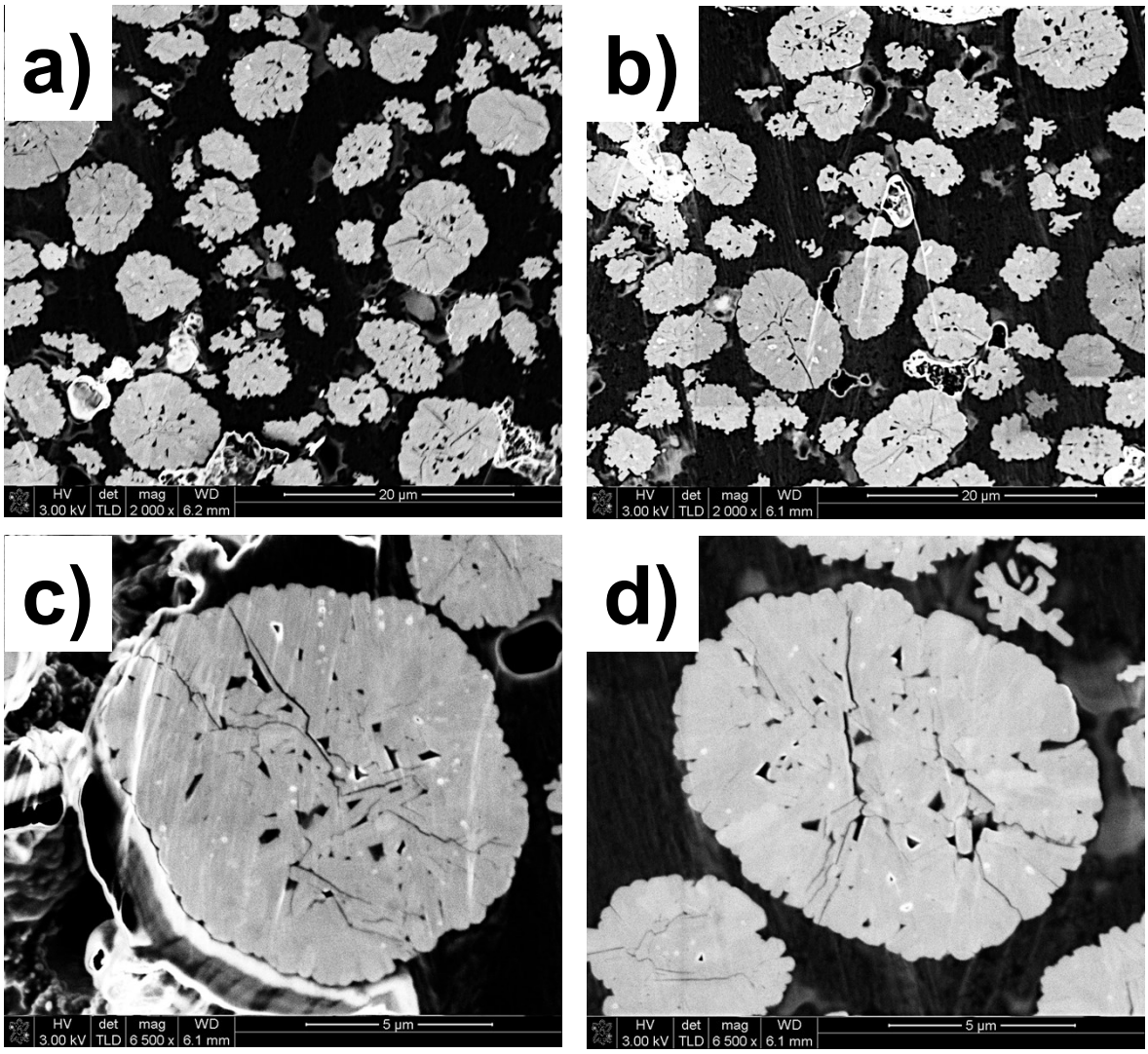

Figure S 13: FIB-SEM cross-sectional slices of a-b) the 47-100-1 electrode taken at 1.5 k× and c-d) two particles taken at 8 k×.

2.5. Outlying Single Particle Analysis

Figure S 14 presents a particle extracted from 47-100-2 with outlying lattice parameter compared to the bulk of the electrode.

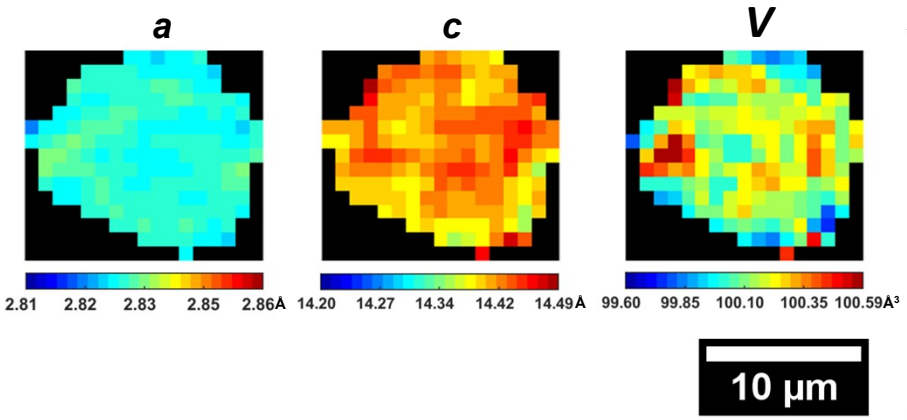

Figure S 14: NMC particle extracted from 47-100-2 with varying lattice parameter compared to bulk electrode.